Cancer Cell
Article

Itraconazole and Arsenic Trioxide Inhibit Hedgehog Pathway Activation and Tumor Growth Associated with Acquired Resistance to Smoothened Antagonists

James Kim,[1,3,10,11] Blake T. Aftab,[5,6,10,12] Jean Y. Tang,[2,9] Daniel Kim,[1,2] Alex H. Lee,[2,9] Melika Rezaee,[9] Jynho Kim,[1,3,4] Baozhi Chen,[8] Emily M. King,[6] Alexandra Borodovsky,[7] Gregory J. Riggins,[7] Ervin H. Epstein, Jr.,[9] Philip A. Beachy,[1,3,4,*] and Charles M. Rudin[6,*]

[1]Institute for Stem Cell Biology and Regenerative Medicine
[2]Department of Dermatology
[3]Departments of Biochemistry and of Developmental Biology
[4]Howard Hughes Medical Institute
Stanford University, Stanford, CA 94305, USA
[5]Department of Pharmacology and Molecular Sciences
[6]Department of Oncology
[7]Department of Neurosurgery
The Johns Hopkins University School of Medicine, Baltimore, MD 21231, USA
[8]Hamon Center for Therapeutic Oncology Research, University of Texas Southwestern, Dallas, TX 75390-8593, USA
[9]Children's Hospital Oakland Research Institute, Oakland, CA 94609, USA
[10]These authors contributed equally to this work
[11]Present address: Division of Hematology-Oncology, Hamon Center for Therapeutic Oncology Research, University of Texas Southwestern, Dallas, TX 75390-8593, USA
[12]Present address: Helen Diller Comprehensive Cancer Center, University of California at San Francisco, San Francisco, CA 94158, USA
*Correspondence: pbeachy@stanford.edu (P.A.B.), rudin@jhmi.edu (C.M.R.)
http://dx.doi.org/10.1016/j.ccr.2012.11.017

SUMMARY

Recognition of the multiple roles of Hedgehog signaling in cancer has prompted intensive efforts to develop targeted pathway inhibitors. Leading inhibitors in clinical development act by binding to a common site within Smoothened, a critical pathway component. Acquired Smoothened mutations, including SMO^{D477G}, confer resistance to these inhibitors. Here, we report that itraconazole and arsenic trioxide, two agents in clinical use that inhibit Hedgehog signaling by mechanisms distinct from that of current Smoothened antagonists, retain inhibitory activity in vitro in the context of all reported resistance-conferring Smoothened mutants and GLI2 overexpression. Itraconazole and arsenic trioxide, alone or in combination, inhibit the growth of medulloblastoma and basal cell carcinoma in vivo, and prolong survival of mice with intracranial drug-resistant SMO^{D477G} medulloblastoma.

INTRODUCTION

The Hedgehog (Hh) signaling pathway is critical for embryonic patterning (Varjosalo and Taipale, 2008) and functions postnatally in tissue homeostasis through its action on stem or progenitor cells (Beachy et al., 2004; Shin et al., 2011). Aberrant Hh signaling has been implicated in oncogenesis, maintenance of tumor progenitor cells, and tumor-stromal interaction in a diverse array of cancers, including tumors that arise sporadically or from individuals with heritable pathway mutations (Teglund and

Significance

Small molecule Hedgehog pathway antagonists currently being evaluated in cancer clinical trials act by binding Smoothened in a manner competitive with cyclopamine. Resistance to these cyclopamine mimics caused by acquired mutations in Smoothened has been described in relevant animal models and in patients. Itraconazole and arsenic trioxide, two readily available FDA-approved drugs with well-defined pharmacokinetics and relatively mild toxicity profiles, have activity in the context of wild-type or resistant Smoothened mutants, in vitro and in vivo. Itraconazole and arsenic trioxide are active Hedgehog pathway inhibitors that could be introduced rapidly into clinical trials for the treatment of de novo Hedgehog-dependent tumors and those with acquired resistance to Smoothened inhibitors.

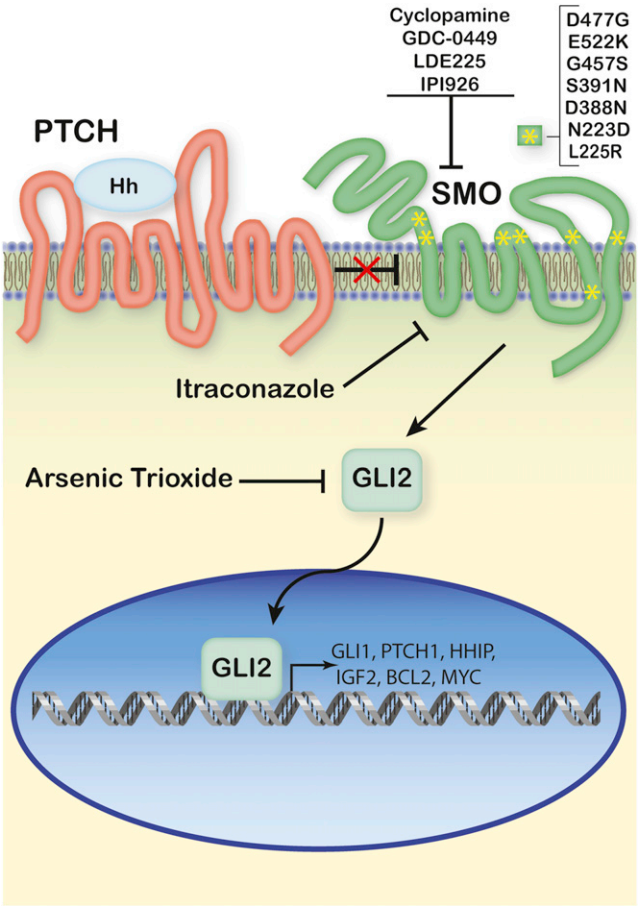

Figure 1. A Simplified View of Hh Signaling

Binding of a Hh ligand to Patched (PTCH) derepresses SMO, causing activation and translocation to the nucleus of GLI2, which initiates the transcription of target genes, including *PTCH* and *GLI1*. Cyclopamine, its derivative, IPI-926, and its mimics, GDC-0449 and NVP-LDE225, all bind competitively to a site within the transmembrane portion of SMO; the SMO missense mutations indicated by yellow asterisks decrease binding and confer resistance to these drugs. Itraconazole inhibits SMO by a distinct mechanism, and ATO inhibits the pathway at the level of GLI.

Toftgård, 2010). This has led to large-scale efforts by multiple pharmaceutical companies to develop Hh pathway antagonists for therapeutic use.

Hh pathway activity is regulated by Patched (PTCH), a 12-pass transmembrane protein that suppresses the activity of Smoothened (SMO), a 7-pass transmembrane protein that traffics constitutively through the primary cilium (Kim et al., 2009; Ocbina and Anderson, 2008). Upon binding of an Hh protein ligand to PTCH, this suppression is relieved, leading to SMO activation and accumulation in the primary cilium (Corbit et al., 2005; Kim et al., 2009; Rohatgi et al., 2007). The GLI2 transcription factor, which also traffics through the cilium, consequently is activated and translocates to the nucleus (Kim et al., 2009), where it activates transcription of Hh-dependent target genes, including *PTCH1* and *GLI1* (Figure 1).

The first Hh-dependent tumors were described in patients with Gorlin syndrome (Gorlin, 1987) (also called basal cell nevus syndrome), an autosomal dominant condition associated with germline loss of one copy of the *PTCH1* gene (Gailani et al., 1992; Hahn et al., 1996; Johnson et al., 1996). The most common tumors arising in these patients are basal cell carcinoma (BCC) of the skin, medulloblastoma (MB), and, more rarely, rhabdomyosarcoma (Gorlin, 1987). Hh pathway upregulation has been found in essentially all cases of BCC (Epstein, 2008), including sporadic BCC, with ~90% containing *PTCH1* mutations (Aszterbaum et al., 1998; Gailani et al., 1996) and ~10% containing activating mutations in *SMO* (Reifenberger et al., 1998; Xie et al., 1998). Hh-dependent MB (Goodrich et al., 1997; Mao et al., 2006) accounts for approximately one-third of all MB (Monje et al., 2011) and is associated with intermediate prognosis (Cho et al., 2011; Ellison et al., 2011; Northcott et al., 2011).

SMO, as a central regulator of the pathway and an accessible cell membrane component, has been the primary focus in the development of small molecule Hh pathway inhibitors. Cyclopamine, the archetypical SMO antagonist, was first described as a steroidal alkaloid teratogen from the corn lily associated with cyclopic lambs (Keeler and Binns, 1966; Keeler and Binns, 1968), and was later determined to be a SMO antagonist (Chen et al., 2002; Cooper et al., 1998; Taipale et al., 2000). Of the many SMO inhibitors in development, four have progressed into phase II trials, including vismodegib (GDC-0449; Genentech), NVP-LDE225 (Novartis), IPI-926 (Infinity), and XL-139 (BMS/Exelixis); IPI-926 is derived from cyclopamine, and all of these inhibitors compete with cyclopamine binding to SMO (S.B. Gendreau and J. Fargnoli, 2009, Mol. Cancer Ther., abstract; Pan et al., 2010; Robarge et al., 2009; Tremblay et al., 2009). GDC-0449 was recently approved for use as a first-line therapy in advanced unresectable BCC (Jefferson, 2012).

The limited mechanistic diversity represented by clinically developed Hh pathway inhibitors has become a focus of clinical concern due the emergence of resistant SMO mutants. The first case of SMO antagonist resistance was reported in a patient with metastatic MB initially highly responsive to GDC-0449 (Rudin et al., 2009). Gene sequencing of recurrent, drug-resistant tumors from this patient identified a SMO missense mutation, D473H, that decreased the binding affinity of GDC-0449 by 100-fold. A homologous mouse mutation, D477G, was found in resistant murine $Ptch^{+/-};p53^{-/-}$ MB generated in vivo by repetitive cycles of treatment with GDC-0449 (Yauch et al., 2009). Another GDC-0449-resistant mutant, E518K, subsequently was identified in human SMO (Dijkgraaf et al., 2011). Development of in vivo resistance to another SMO antagonist, NVP-LDE225, was demonstrated in murine MB, with mutations occurring at residues L225, N223, S391, D388, and G457 (Buonamici et al., 2010). The latter reports also identified other putative mechanisms of resistance, including *Gli2* and *Ccnd1* amplification, and activation of the PI3K-AKT-mTOR signaling pathway.

We have previously identified itraconazole, an FDA-approved triazole antifungal agent, and arsenic trioxide (ATO), which is FDA-approved for the treatment of acute promyelocytic leukemia (APL), as potent inhibitors of the Hh pathway (Kim et al., 2010a; Kim et al., 2010b). Itraconazole inhibits Hh pathway activation at the level of SMO at a site distinct from that of cyclopamine mimics currently in development, and by

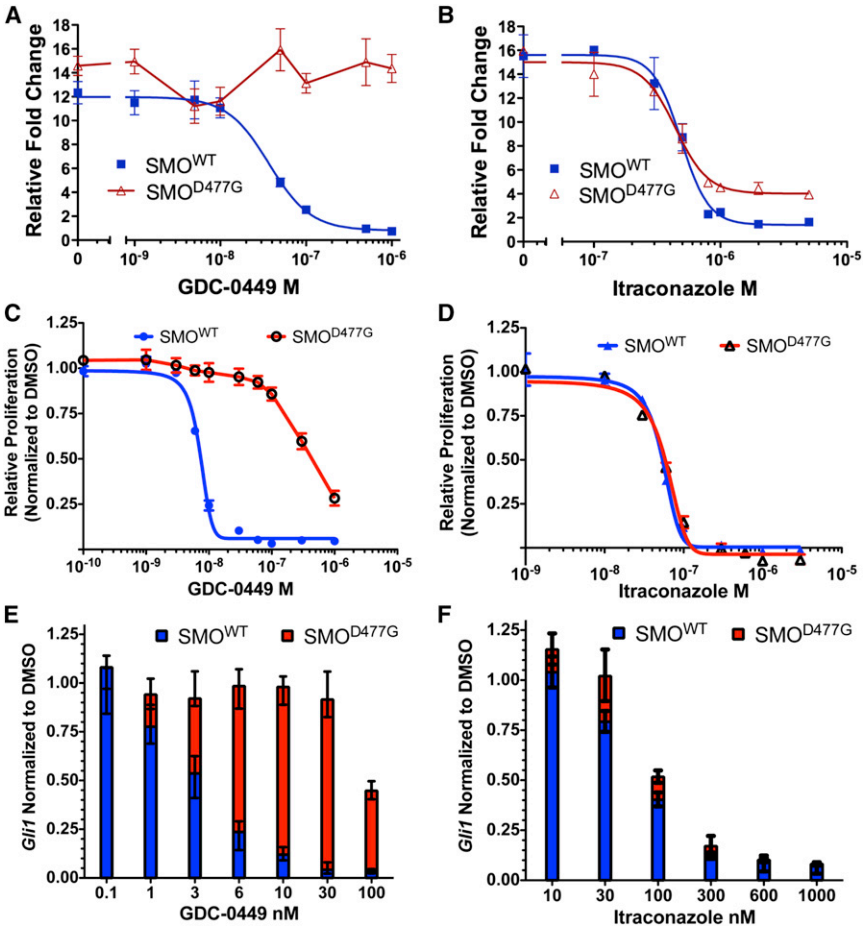

Figure 2. Itraconazole Inhibits the Hh Pathway in the Context of GDC-0449 Resistant SMO^{D477G}

(A and B) Relative Hh pathway activity as determined by expression of 8×-GLI-luciferase reporter in SHH-N stimulated *Smo*$^{-/-}$ MEFs expressing SMO^{WT} (blue) or SMO^{D477G} (red) treated with (A) GDC-0449 or (B) itraconazole. Data represent mean of triplicates ± SD.

(C and D) Proliferation of *Ptch*$^{+/-}$; *p53*$^{-/-}$ MB tumorspheres expressing endogenous SMO^{WT} (blue) or SMO^{D477G} (red) treated with increasing doses of (C) GDC-0449 and (D) itraconazole. Data represent mean of quadruplicates ± SEM.

(E and F) Relative *Gli1* mRNA transcription in (C) GDC-0449-treated and (D) itraconazole-treated MB tumorspheres expressing endogenous SMO^{WT} (blue) or SMO^{D477G} (red). Data represent mean of quadruplicates ± SEM.

See also Figure S1.

a mechanism distinct from its antifungal target of lanosterol-14α demethylase (Kim et al., 2010b).

ATO directly binds to the zinc finger motif of the promyelogenous leukemia-retinoic acid receptor fusion protein (PML-RARα), the causative factor of APL (de Thé et al., 1990, 1991; Rowley et al., 1977), and promotes its degradation (Lallemand-Breitenbach et al., 2008; Zhang et al., 2010). Similarly, ATO inhibits Hh signaling by inhibiting GLI2 ciliary accumulation and promoting its degradation (Kim et al., 2010a). ATO also inhibited the growth of Ewing Sarcoma tumors overexpressing *GLI1* due to direct transcriptional activation by the EWS-FLI1 fusion oncoprotein (Beauchamp et al., 2009, 2011; Joo et al., 2009; Zwerner et al., 2008).

The occurrence of drug-resistant SMO mutations highlights the therapeutic need for agents capable of maintaining robust on-target clinical responses. Small molecule compounds that overcome resistance to murine SMO^{D477G} (Dijkgraaf et al., 2011; Tao et al., 2011) or human SMO^{D473H} (Dijkgraaf et al., 2011) have been reported recently, but with no clear timeline for clinical development. As FDA-approved drugs, itraconazole and ATO represent readily available agents with distinct modes of Hh pathway inhibitory activity. Therefore, we sought to test the efficacy of itraconazole and ATO, as single agents and in combination, to inhibit Hh pathway activity and growth of tumors with drug-resistant SMO mutations.

RESULTS

Itraconazole Inhibits GDC-0449-Resistant Pathway Activity Mediated by SMO^{D477G}

Because itraconazole acts on SMO at a site distinct from that of cyclopamine and cyclopamine mimics (Kim et al., 2010b), we hypothesized that itraconazole may have activity against the GDC-0449 resistance mutant, SMO^{D477G} (Yauch et al., 2009). First, we evaluated the ability of itraconazole to inhibit Hh pathway activity in the context of SMO^{WT} or SMO^{D477G} expression. *Smo*^{WT} or *Smo*^{D477G} were cotransfected with 8 × -GLI binding site firefly luciferase and SV40-Renilla reporters (Taipale et al., 2000) into a *Smo*$^{-/-}$ mouse embryonic fibroblast (MEF) cell line (Varjosalo et al., 2006) and treated with SHH-N conditioned medium (CM) (Maity et al., 2005). As expected, GDC-0449 was active against SMO^{WT}, but unable to inhibit SMO^{D477G} (Figure 2A). In contrast, itraconazole potently inhibited both SMO^{WT} and SMO^{D477G} (Figure 2B), although the maximal inhibition of SMO^{D477G} activity up to a concentration of 5 μM itraconazole left a residual ~30% activity (Figure 2B). Itraconazole thus acts as a full antagonist of SMO^{WT} and as a partial antagonist of SMO^{D477G}. Similar to human SMO^{D473H} (Yauch et al., 2009), murine SMO^{D477G} was less susceptible to inhibition by KAAD-cyclopamine, as evidenced by the rightward shift of the mutant dose-response curve (Figure S1A available online). However, unlike GDC-0449, KAAD-cyclopamine was able to fully inhibit SMO^{D477G} activity at higher doses.

To evaluate itraconazole activity against Hh-dependent tumors, we tested the ability of itraconazole to inhibit pathway activity in tumorsphere cultures established using MB cells with constitutive Hh pathway activity from *Ptch*$^{+/-}$;*p53*$^{-/-}$ mice (Berman et al., 2002; Goodrich et al., 1997; Romer et al., 2004). When cultured in neural stem cell medium, these cells grow in an Hh pathway-dependent manner and form

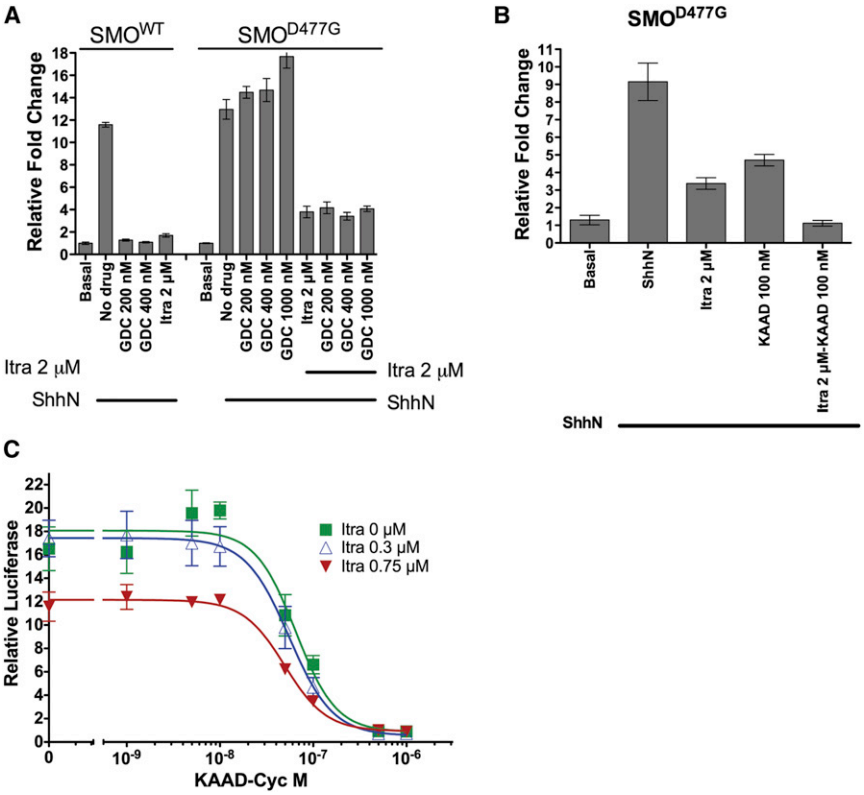

Figure 3. Itraconazole Combines with Cyclopamine to Inhibit GDC-0449-Resistant SMO Function

(A) Relative 8×-GLI-luciferase expression in SHH-N-stimulated *Smo*$^{-/-}$ MEFs expressing SMO^{WT} or SMO^{D477G}, treated with GDC-0449, itraconazole, or both.

(B) Effect of KAAD-cyclopamine 100 nM, itraconazole 2 μM, or both on SHH-N-stimulated 8×-GLI-luciferase expression in *Smo*$^{-/-}$ MEFs expressing SMO^{D477G}.

(C) Dose-response curves of KAAD-cyclopamine for SHH-N activated signaling in *Smo*$^{-/-}$ MEFs expressing SMO^{D477G}, in the presence or absence of itraconazole. All data represent mean of triplicates ± SD.

See also Figure S2 and Table S1.

tumorspheres maximally enriched for the highly tumorigenic CD-15^{+} cell population (Ward et al., 2009) (Read et al., 2009; Shi et al., 2011). We utilized tumorsphere cultures derived from allografts of parental SMO^{WT} and derivative SG274 MB cells that express spontaneously acquired SMO^{D477G} (Dijkgraaf et al., 2011; Yauch et al., 2009) to examine the differential potency of itraconazole in an endogenous system of drug resistance. The SMO^{D477G}-expressing tumorspheres were ~100-fold less sensitive than parental SMO^{WT} tumorspheres to antiproliferative activity of GDC-0449 by MTS analysis (Figure 2C). In this system, itraconazole displayed equivalent antiproliferative activity in the parental (IC_{50} 55 nM; 50–60 nM confidence interval [CI]) and SMO^{D477G} mutant MB cells (62 nM; 53–70 nM CI) (Figure 2D). Inhibition of Hh pathway activity, as monitored by *Gli1* mRNA levels, correlated with the antiproliferative potencies of GDC-0449 (Figure 2E) and itraconazole (Figure 2F). In contrast to the *Smo*$^{-/-}$ MEF reporter-based signaling assay, itraconazole fully inhibited proliferation and Hh pathway activity in the *SMO*^{WT} and GDC-0449-resistant MB cultures. MB spheres also were more sensitive to itraconazole, with ~100 nM IC_{50} for *Gli1* mRNA transcription compared to ~600 nM IC_{50} for the luciferase reporter assay in *Smo*$^{-/-}$ MEFs. HhAntag (Gabay et al., 2003; Romer et al., 2004), a SMO antagonist structurally distinct from GDC-0449 and cyclopamine, has been reported to inhibit SMO^{D473H} at 1 μM (~25 × IC_{50} for SMO^{WT}) (Dijkgraaf et al., 2011). Pathway inhibition by HhAntag, as measured by *Gli1* mRNA, showed a similar behavior to that of KAAD-cyclopamine (Figure S1A), in that its inhibition curve shifts to the right (Figure S1B). The decrease in potency of HhAntag and KAAD-cyclopamine in the context of SMO^{D477G} is consistent with previous reports for other inhibitors that compete for cyclopamine binding to SMO (Dijkgraaf et al., 2011; Lee et al., 2012).

Combination of Itraconazole and Cyclopamine Can Inhibit SMO^{D477G}

Because we previously showed that itraconazole and KAAD-cyclopamine synergize to inhibit SMO^{WT} (Kim et al., 2010b) and that these drugs act at distinct sites (Kim et al., 2010b), we hypothesized that itraconazole might also act synergistically with cyclopamine mimics to inhibit the activity of SMO^{D477G}. We found, however, that addition of GDC-0449 did not enhance itraconazole inhibitory potency against SMO^{D477G}, suggesting that GDC-0449 does not contribute to pathway suppression in the combination (Figure 3A). Combination of itraconazole and KAAD-cyclopamine completely inhibited SMO^{D477G} activity at doses that are partially inhibitory for the individual agents (Figure 3B). The addition of itraconazole to KAAD-cyclopamine did not shift the IC_{50} of KAAD-cyclopamine (Figure 3C; Figure S2; Table S1), suggesting that the two drugs inhibit SMO^{D477G} additively.

Itraconazole and Arsenic Trioxide Combine to Inhibit Hh Pathway Activity and Tumor Growth

Because ATO inhibits the Hh pathway at the level of GLI proteins (Kim et al., 2010a) and itraconazole acts on SMO, we hypothesized that the two drugs might synergize in pathway inhibition. We tested the drug combination against SMO^{WT} in transiently transfected NIH 3T3 cells using fixed doses of one drug while titrating the other. The combination of itraconazole and ATO improves Hh pathway inhibition (Figures 4A and 4B), but this effect appears additive rather than synergistic, because there is no leftward shift of IC_{50} for either drug (Figures 4A and 4B; Figures S3A and S3B; Tables S2 and S3).

We next tested the itraconazole/ATO combination in tumor growth inhibition in vivo using a subcutaneous allograft model of *Ptch*$^{+/-}$;*p53*$^{-/-}$ mouse MB. Nude mice with established tumors were treated with intraperitoneal (i.p.) ATO 7.5 mg/kg once daily, or oral itraconazole 75 mg/kg twice daily, or

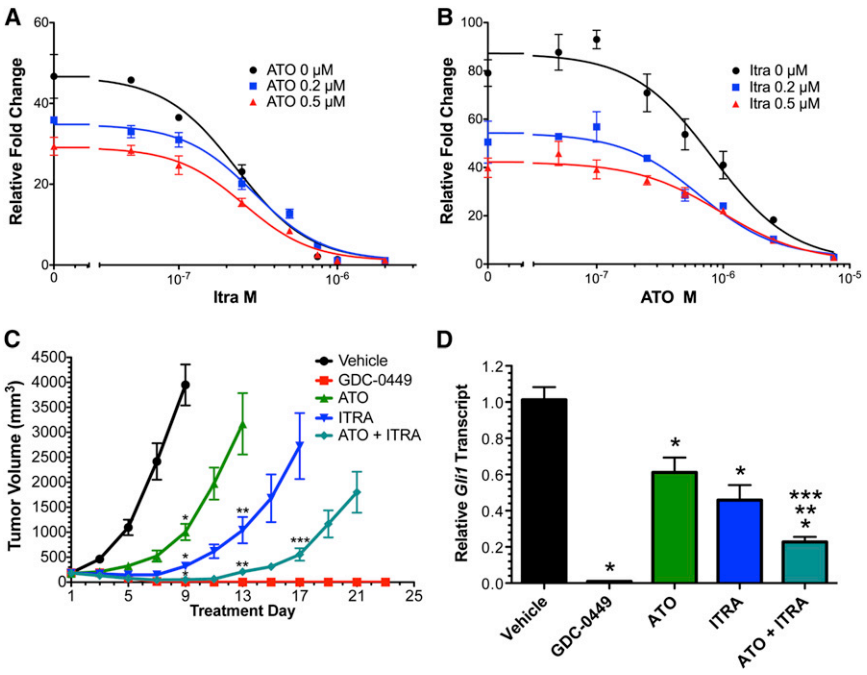

Figure 4. ATO and Itraconazole Combine to Inhibit Hh Pathway Activation and Tumor Growth by SMO^{WT}

(A and B) Effect of combination therapy on the IC_{50} concentrations of itraconazole (A) or ATO (B) in NIH 3T3 cells expressing endogenous SMO^{WT} stimulated with SHH-N in 8×-GLI-luciferase signaling assays. Data represent mean of triplicates ± SD.

(C and D) Nude mice with SMO^{WT} hindflank MB allografts were treated with vehicle control (40% cyclodextrin orally twice daily, n = 7 tumors; black), GDC-0449 (100 mg/kg orally twice daily, n = 7; red), ATO (7.5 mg/kg i.p. once daily, n = 7 tumors; green), itraconazole (75 mg/kg orally twice daily, n = 7 tumors; blue), or both ATO and itraconazole (n = 7 tumors; blue-green). Effect of GDC-0449, ATO, itraconazole, or the combination of ATO and itraconazole on (C) tumor growth and (D) *Gli1* mRNA expression compared to vehicle control. Data represent group means ± SEM (*p < 0.01 versus vehicle; **p < 0.01 versus ATO alone; ***p < 0.01 versus itraconazole alone).

See also Figure S3 and Tables S2 and S3.

a combination of both drugs. Single-agent therapy with ATO or itraconazole significantly inhibited tumor growth (Figure 4C), and was associated with 78% ($p < 0.005$) and 96% ($p < 0.001$) growth inhibition, respectively, as compared to vehicle-treated tumors on day 9 of treatment. During the same vehicle-controlled time period, the combination of ATO and itraconazole not only inhibited tumor growth, but also reduced tumor volumes by 72% from the start of treatment ($p < 0.001$ versus vehicle; $p < 0.001$ versus initial volumes). Combination treatment compared to ATO or itraconazole alone significantly improved antitumor efficacy, with 99% and 85% inhibition of tumor growth relative to ATO or itraconazole alone through the single-agent controlled portions of study, on days 13 and 17, respectively (Figure 4C; $p < 0.001$ for both). ATO and itraconazole were well tolerated, both as single agents and in combination, as body weights were similarly maintained across cohorts (Figure S3C).

Inhibition of MB tumor growth was associated with parallel reductions in Hh pathway activity in treated tumors (Figure 4D). Compared to vehicle-treated tumors, single-agent ATO or itraconazole treatment resulted in 39% and 55% inhibition of tumor *Gli1* mRNA expression, respectively ($p < 0.01$ for both), whereas combined ATO and itraconazole suppressed tumor *Gli1* mRNA transcript levels by 77% ($p < 0.001$ versus vehicle and ATO alone; $p < 0.01$ versus itraconazole alone).

We also monitored the status of the PI3K pathway and *GLI2* in the treated tumors (Figures S3D–S3F), because PI3K pathway activation and *GLI2* amplification and overexpression have been reported as mechanisms of resistance to cyclopamine-competitive antagonists (Buonamici et al., 2010; Dijkgraaf et al., 2011). Tumors with Hh pathway inhibition (Figure 4D) displayed a low level of PI3K pathway activation at baseline, evidenced by phosphorylation of AKT, S6K, and 4E-BP1 (reviewed in Cully et al., 2006) that was largely unchanged in response to the single-agent or combination treatments (Figure S3D). Tumors that eventually progressed during drug therapy (Figure 4C) did not show increased levels of pAKT and pS6K (Figure S3E), nor did they display increased *Gli2* mRNA (Figure S3F). These results suggest that the previously described mechanisms of resistance to GDC-0449 and LDE225 are not the cause of eventual tumor growth with itraconazole and ATO treatment, which more likely is caused by incomplete, albeit substantial, pathway suppression.

Additionally, in a subcutaneous allograft model of BCC derived from *Ptch$^{+/-}$;K14-Cre$^{ER2/+}$;p53$^{fl/fl}$* mice (Tang et al., 2011), the combination of itraconazole and ATO significantly inhibited tumor growth compared to control ($p < 0.001$ at day 30 of treatment) (Figure 5). Mice treated with single agents displayed reductions in mean tumor growth that did not reach statistical significance compared to control.

Combination of Itraconazole and ATO Can Inhibit Hh Pathway Activity Mediated by GDC-0449-Resistant SMO In Vitro and In Vivo

Having established efficacy of the itraconazole/ATO combination for antagonism of SMO^{WT} activity in vitro and in vivo, we tested the combination against the GDC-0449-resistant SMO mutant, SMO^{D477G} (Yauch et al., 2009). We previously showed that ATO can inhibit SMO^{D477G} activity (Kim et al., 2010a). In SHH-N-stimulated *Smo$^{-/-}$* MEFs transfected with *Smo^{D477G}*, addition of ATO to itraconazole inhibited Hh pathway activation in a dose-dependent fashion (Figure 6A) and led to improved inhibition by itraconazole at higher doses (Figure 6B), indicating a greater potency for the combination. Similar to SMO^{WT} (Figures 4A and 4B), ATO and itraconazole inhibited SMO^{D477G} activity additively (Figure 6C; Figure S4A; Table S4), with no leftward IC_{50} shift (Figure S4A; Table S4).

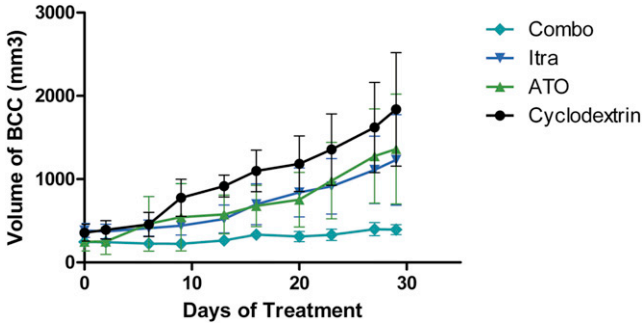

Figure 5. Combination of ATO and Itraconazole Inhibits Tumor Growth of Hh-Dependent BCC

NOD/SCID mice with established *K14-Cre$^{ER/+}$;Ptch$^{+/-}$;p53$^{fl/fl}$* BCC allografts were treated with vehicle control (40% cyclodextrin orally twice daily, n = 4 tumors; black), ATO (7.5mg/kg i.p. once daily, n = 6 tumors; green), itraconazole (75 mg/kg orally twice daily, n = 10 tumors; blue), or both ATO and itraconazole (n = 16 tumors; blue-green; $p < 0.01$ for the combination compared to either itraconazole or ATO alone). Data represent group means ± SEM.

We tested combination treatment in vivo in a GDC-0449-resistant *Ptch$^{+/-}$;p53$^{-/-}$* murine MB allograft model expressing endogenous SMO^{D477G} (Yauch et al., 2009). In contrast to the results observed in SMO^{WT} tumors (Figure 4C), twice-daily treatment with GDC-0449 did not significantly impact tumor growth or Hh pathway status compared to control (Figures 6D and 6E). Of note, a similar albeit less dramatic differential was associated with once-daily treatment with HhAntag treatment in this model (Figures S4B–S4D). Unlike GDC-0449, ATO and itraconazole inhibited SMO^{D477G} MB growth with similar potency to that of SMO^{WT} tumors. In GDC-0449-resistant tumors, single-agent ATO and itraconazole resulted in 78% and 92% growth inhibition, respectively, versus control through the 9-day vehicle-controlled period ($p < 0.001$ for both). Combination treatment over the same period completely inhibited tumor growth and caused 48% tumor regression from the start of study ($p < 0.001$ versus vehicle; versus initial volumes). Furthermore, the efficacy of the combination was superior to either agent alone, and resulted in 97% relative tumor growth inhibition over ATO alone ($p < 0.001$) and 85% improvement over itraconazole alone ($p < 0.001$) through the 12-day period controlled by the respective single-agent arms (Figure 6D).

Treated tumors revealed that single-agent itraconazole and ATO inhibited Hh pathway activity in GDC-0449-resistant allografts (Figure 6E) with similar magnitudes of 43% and 45% of control-treated tumors, respectively, as measured by *Gli1* mRNA transcript ($p < 0.01$ for both). Combination treatment resulted in further pathway suppression to 66% ($p < 0.01$). *Gli1* mRNA expression was not significantly inhibited ($p > 0.05$) in response to GDC-0449.

The hindflank allograft model of SMO^{D477G} MB serves as a valuable proxy for antitumor potential in the context of GDC-0449 resistance. However, the ectopic nature of this model fails to account for the challenges of treating an advanced intracranial malignancy. To further evaluate the potential clinical relevance of itraconazole and ATO in MB treatment, we assessed survival in an orthotopic model of SMO^{D477G} MB. Survival of mice bearing engrafted intracranial tumors did not improve with GDC-0449, because both treatment and control resulted in median survival times of 14 days (Figure 6F, red and black lines, respectively; $p = 0.69$). In contrast, survival of mice receiving single-agent treatment with ATO or itraconazole (Figure 6F, green or blue lines, respectively) improved significantly over control, with median survival times of 18 days ($p = 0.0041$) and 22 days ($p = 0.0001$). The combination of these drugs (Figure 6F, blue-green line) further improved survival over either single-agent alone ($p \leq 0.0001$) and doubled the survival time over GDC-0449 and vehicle arms, with a median survival of 29 days ($p < 0.0001$ compared to vehicle or GDC-0449 arms).

Combination of Itraconazole and ATO Remains Active in All Known Drug-Resistant SMO Mutations and in the Context of GLI2 Overexpression

In addition to SMO^{D473H} (murine SMO^{D447G}), alanine scan mutagenesis identified potential alterations of SMO^{E518} that confer resistance to GDC-0449 (Dijkgraaf et al., 2011). Five resistance mutants to another SMO antagonist, NVP-LDE225, have also been reported in *Ptch$^{+/}$;p53$^{-/-}$* and *Ptch$^{+/-}$;Hic1$^{+/-}$* MB models (Buonamici et al., 2010). We transiently transfected these drug-resistant *Smo* mutants into *Smo$^{-/-}$* MEFs and induced pathway activation with SHH-N CM. Cells were treated with GDC-0449 0.5 μM (~40 × IC_{50}; Robarge et al., 2009), NVP-LDE225 0.5 μM (~80 × IC_{50}; Buonamici et al., 2010), itraconazole 1.5 μM, ATO 2.5 μM, and a combination of itraconazole and ATO. We confirmed previously reported resistance of the various SMO mutants (Figure 7), including partial sensitivity of Smo^{G457S} to NVP-LDE225 (Figure 7C) consistent with an IC_{50} of 400 nM (Buonamici et al., 2010). Smo^{G457S} was, however, resistant to 50 nM NVP-LDE225 (~8 × IC_{50} of SMO^{WT}; Figure 7C).

Itraconazole inhibited activity of all known SMO resistance mutants at similar levels to SMO^{D477G} (Figure 7), except for murine SMO^{E522K}, which corresponds to human SMO^{E518}. SMO^{E522K} was resistant to GDC-0449 and, unlike SMO^{D477G}, was almost completely inhibited by itraconazole (Figure 7B). Itraconazole 1.5 μM inhibited the NVP-LDE225-resistant mutants (Figures 7C–7G), with a range of ~40% (Figure 7C) to ~60% (Figure 7D). The addition of ATO 2.5 μM to itraconazole was able to completely inhibit the activity of these mutants. As expected, higher doses of ATO completely inhibited all of the resistant mutants (Figure S5), because ATO acts downstream of SMO.

We previously showed that ATO inhibits the Hh pathway through inhibition of ciliary transport and degradation of the GLI proteins (Kim et al., 2010a). We tested itraconazole and ATO, alone and in combination, on NIH 3T3 cells that ectopically overexpressed GLI2 with and without the addition of SHH-N CM (Figure 7H). GLI2 overexpression alone caused elevated pathway activity, and the addition of SHH-N CM further induced Hh pathway activation. As expected, itraconazole inhibited pathway activity induced by SHH-N but not by GLI2 overexpression (Figure 7H), because itraconazole acts upstream of GLI2 (Kim et al., 2010b). ATO, however, was able to inhibit pathway activity induced by SHH-N and GLI2. The combination of itraconazole and ATO inhibited pathway activity induced by both SHHN and GLI2 overexpression to a similar extent as was observed with ATO alone.

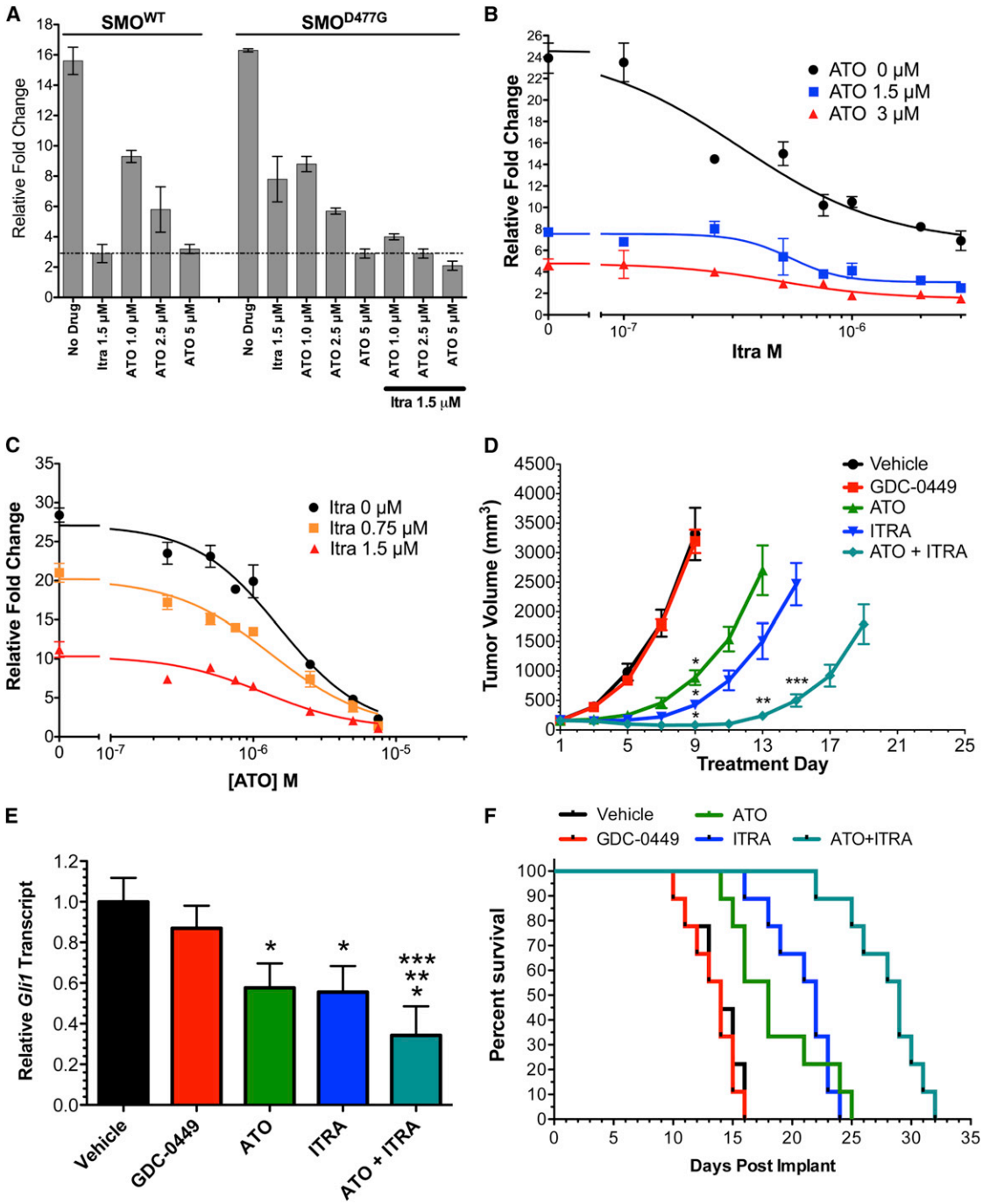

Figure 6. ATO and Itraconazole Combine to Inhibit SMO^{D477G} Activity and Tumor Growth, and Improve Survival in an Orthotopic Medulloblastoma Model

(A–C) *Smo*$^{-/-}$ MEFs were transfected with either *Smo*^{WT} *or Smo*^{D477G} and stimulated with SHH-N. Data represent mean of triplicates ± SD. (A) Relative Hh pathway activity as assessed by relative 8 × -GLI-luciferase expression in the presence or absence of itraconazole, ATO, or the combination. Dashed line represents the level of pathway inhibition of SMO^{WT} by itraconazole 1.5 μM. (B) Effect of the addition of increasing doses of ATO to itraconazole in cells expressing SMO^{D477G}. (C) Effect of increasing doses of itraconazole on the IC_{50} of ATO in cells expressing SMO^{D477G}.

(D and E) Nude mice with established SMO^{D477G} MB allografts were treated with vehicle control (40% cyclodextrin orally twice daily, n = 8 tumors; black), GDC-0449 (100 mg/kg orally twice daily, n = 8; red); ATO (7.5mg/kg i.p. once daily, n = 8 tumors; green), itraconazole (75 mg/kg orally twice daily, n = 8 tumors; blue), or both ATO and oral itraconazole (n = 8 tumors; blue-green); (D) tumor growth over time and (E) relative *Gli1* mRNA expression. Data represent group means ± SEM (*p < 0.01 versus vehicle; **p < 0.01 versus ATO alone; ***p < 0.01 versus ITRA alone).

(F) Kaplan-Meier survival analysis of an orthotopic model of SMO^{D477G} MB treated with vehicle control (n = 9), GDC-0449 (n = 9), itraconazole (n = 9), ATO (n = 9), or both ATO and itraconazole (n = 9) using the same doses as in (D).

See also Figure S4 and Table S4.

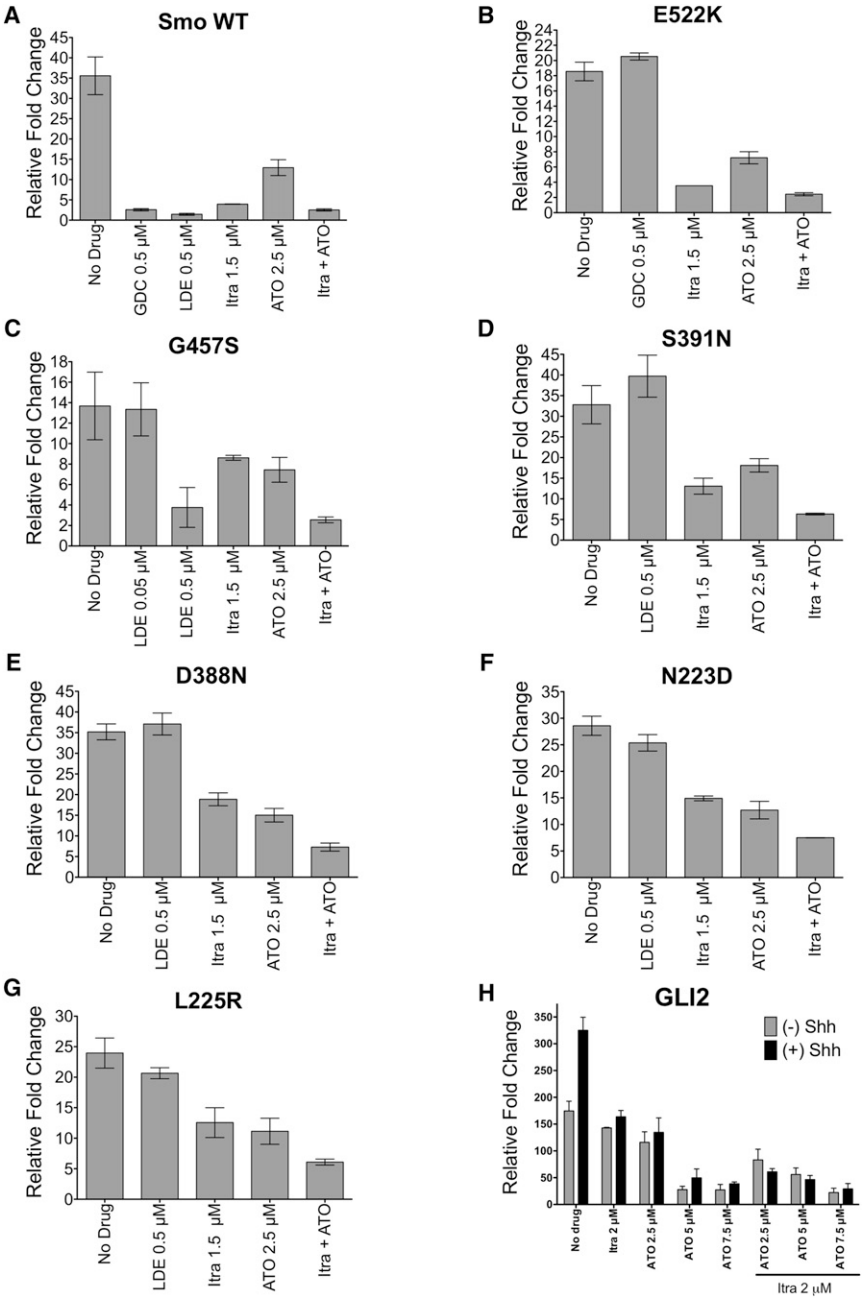

Figure 7. Combination of ATO and Itraconazole Inhibits All Other Known Drug-Resistant SMO Mutants and GLI2 Overexpression

(A–G) SHH-N stimulated $Smo^{-/-}$ MEFs were transfected with (A) Smo^{WT} or mutant Smo constructs resistant to (B) GDC-0449 or (C–G) NVP-LDE225. The effects of itraconazole, ATO, and the combination of both agents on Hh pathway activity was assessed by relative 8×-GLI-luciferase activity. Labels in (B–G) indicate the mutant SMO that was expressed.

(H) Effect of itraconazole, ATO, or the combination on relative 8×-GLI-luciferase activity in NIH 3T3 cells transfected with *Gli2* ± SHH-N stimulation. Data represent mean of triplicates ± SD.

See also Figure S5.

DISCUSSION

Itraconazole, Cyclopamine Mimics, and SMO

Prior to our studies of itraconazole, most or all SMO modulators, including GDC-0449 and NVP-LDE225, were found to compete with BODIPY-cyclopamine for binding to SMO, presumably by binding at closely overlapping sites. Recent studies (Dijkgraaf et al., 2011; Nachtergaele et al., 2012; Tao et al., 2011), however, reveal additional complexity. Tao et al. (2011) show that several recently identified Hh antagonists compete for binding with distinct subsets of BODIPY-cyclopamine competitive Smo modulators, suggesting that the BODIPY-cyclopamine binding pocket and nearby regions within SMO may accommodate two non-overlapping modulators simultaneously. Furthermore, oxysterol agonists that do not compete with BODIPY-cyclopamine (Dwyer et al., 2007) have been shown to bind SMO directly (Nachtergaele et al., 2012), presumably at a distinct site.

Itraconazole appears to act entirely outside the BODIPY-cyclopamine binding pocket, because it fails to compete with BODIPY-cyclopamine or the SMO agonist, SAG (Kim et al., 2010b). We cannot rule out the possibility that itraconazole acts on SMO indirectly via another molecule, because we do not have a direct binding assay. Nonetheless, the ability of itraconazole to inhibit all of the SMO variants resistant to GDC-0449 and NVP-LDE225 is consistent with its action on SMO at a distinct site from that of cyclopamine and its mimics. Although compounds that overcome SMO^{D477G} activity and act within the BODIPY-cyclopamine pocket of SMO have been reported (Dijkgraaf et al., 2011; Tao et al., 2011), their inhibitory activity against other SMO mutations and their toxicity and pharmacological properties in patients remain unknown.

Interestingly, itraconazole only partially inhibits the activity of SMO^{D477G} (Figure 2B) and the other mutants, except for SMO^{E522K} (Figure 7). Small molecule partial antagonists for the GPCR mGlu5 receptor have been described (Lamb et al., 2011; Rodriguez et al., 2005, 2010) that act as noncompetitive allosteric inhibitors of the orthosteric endogenous ligand, glutamate (Wood et al., 2011). By analogy, perhaps itraconazole acts as an allosteric inhibitor of a currently undefined endogenous SMO-interacting factor. The mutant SMO proteins may exist in conformations that allow itraconazole to exert its inhibitory function in an incomplete fashion.

Combination of Itraconazole and ATO as Therapy for Hh-Dependent Tumors

We have shown that itraconazole and ATO, alone and in combination, inhibit Hh pathway activity and growth of in vitro cultured cells and in vivo tumors bearing wild-type and drug-resistant SMO. The eventual, albeit significantly delayed, in vivo tumor growth from itraconazole and ATO treatment is not due to previously described resistance mechanisms of PI3K-mTOR activation or *Gli2* amplification (Figures S3D–S3F). Induction of P-glycoprotein (PGP) and drug efflux, recently reported (Lee et al., 2012) as a resistance mechanism to IPI-926, is unlikely to be the case in our studies because itraconazole is a potent inhibitor of PGP (Wang et al., 2002). The tumor growth kinetics in our studies more likely reflect the incomplete albeit substantial degree of Hh pathway inhibition by itraconazole and ATO; this incomplete inhibition might be improved by adjusting the relative or overall dosages of itraconazole and ATO in the combination. Other mechanisms to account for the eventual tumor regrowth, however, cannot be fully excluded at this time.

Itraconazole also has been reported to inhibit mTOR activity (Xu et al., 2010), and ATO has been reported to upregulate PTEN (Redondo-Muñoz et al., 2010) and degrade AKT (Mann et al., 2008). However, we did not observe significant changes in PI3K pathway activity in our short-term (Figure S3D) or long-term (Figure S3E) analyses. Several reasons may account for the apparent discrepancy. First, the studies cited for the activity of itraconazole and ATO against the PI3K pathway were all performed in cell culture systems with robust activation of the PI3K pathway, and may not accurately reflect the in vivo environment examined here. Second, the marginal detection of PI3K pathway activation in our in vivo tumor models suggest that this pathway contributes little to tumor growth, and that further inhibition by pharmacologic means may not be possible.

The therapeutic regimen of itraconazole and ATO combination is active against all reported functional SMO resistance mutants and has several advantages over single-agent SMO inhibition. In addition to Hh pathway inhibition, itraconazole inhibits angiogenesis through vascular endothelial growth factor and fibroblast growth factor (FGF) blockade (Aftab et al., 2011; Chong et al., 2007; Nacev et al., 2011). Likewise, ATO induces apoptosis by caspase activation, BCL2 inhibition, and reactive oxygen species accumulation, NF-κB inhibition (Emadi and Gore, 2010), and the promotion of GLI protein degradation (Kim et al., 2010a). The combination of itraconazole and ATO simultaneously targets two distinct and critical loci within the Hh pathway: SMO and GLI proteins. Such multifocal targeting within the Hh pathway itself and other pathways necessary for tumor growth may prevent or delay the emergence of resistant tumor clones. Moreover, the additive inhibitory effect of the itraconazole/ATO combination allows for the use of lower doses of each drug to maintain or improve antitumor efficacy while decreasing the likelihood of adverse toxicities. Finally, our data suggest that ATO, alone or in combination with itraconazole, may also inhibit tumor growth associated with GLI2-mediated resistance (Figure 7H; Kim et al., 2010a).

With the recent FDA approval of GDC-0449 for advanced BCC and with multiple other cyclopamine mimics in clinical trials, we anticipate that examples of clinical resistance and other drug-resistant SMO mutants will become more prevalent. This represents a substantial threat to patients and emphasizes the need to identify clinical candidates capable of maintaining on-target efficacy in the face of such mutations. Itraconazole and ATO are both FDA-approved drugs that are well tolerated, readily available, and with well-characterized pharmacokinetic and toxicity profiles. We have shown that the combination of itraconazole and ATO is effective against SMO^{WT}, the recently reported SMO mutants resistant to cyclopamine-mimics, and against GLI2 overexpression. These factors strongly support the clinical evaluation of itraconazole and ATO in the treatment of de novo Hh-dependent tumors or those with acquired resistance to cyclopamine mimics.

EXPERIMENTAL PROCEDURES

Detailed procedures can be found in Supplemental Experimental Procedures.

Reagents

Itraconazole (Sigma), vismodegib (GDC-0449; LC Laboratories), and NVP-LDE225 (LC Laboratories) were dissolved in dimethyl sulfoxide for in vitro experiments. ATO powder (Sigma) for in vitro experiments was formulated as previously described (Zhu et al., 2002). Itraconazole oral solution (Sporanox, Ortho Biotech) and ATO (Trisenox; Cephalon) for in vivo experiments were obtained from the pharmacies of The Johns Hopkins and Stanford Cancer Centers. For in vivo studies, GDC-0449 100 mg/kg oral gavage (twice daily), ATO 7.5mg/kg i.p. (once daily), and itraconazole 75 mg/kg orally (twice daily) were used both as single agents and in combination.

Cell-Based Signaling Assays

Plasmid constructs for Smo^{WT} or Smo^{D477G}, *Gli2* (Kim et al., 2010a), *GFP*, GLI-dependent firefly luciferase reporter, and TK-*Renilla* luciferase reporter (Taipale et al., 2000) have been described previously. Constructs for other Smo resistance mutants were prepared using standard site mutagenesis techniques to pCEFL-Smo^{WT} and verified by DNA sequencing. Fugene 6 (Roche Applied Science) or TransIT (Mirus Bio) reagents were used for transient transfections.

NIH 3T3 cell line (ATCC) and $Smo^{-/-}$ MEF cell line (Varjosalo et al., 2006) were stimulated with SHH-N CM (Maity et al., 2005) or control HEK293 CM for Hh pathway signaling assays.

Cells were incubated for ~40 hr with drug treatments. Relative luciferase (fold induction) units were obtained by normalization of luciferase signals from SHHN CM stimulated with control CM stimulated cells. Luminescence assays were performed on a Fluostar Optima (BMG Labtech) or Centro (Berthold Technologies) using Dual Luciferase Assay Reporter System (Promega).

In Vivo Studies

All mouse studies were approved by and conformed to the policies and regulations of the respective Institutional Animal Care and Use Committees at the Johns Hopkins University and the Children's Hospital Oakland Research Institute.

BCC Allograft Model

Endogenous BCC tumors from $Ptch1^{+/-}$; $K14\text{-}Cre^{ER}$; $p53^{fl/fl}$ mice (Tang et al., 2011) were subcutaneously established as flank xenografts in NOD/SCID mice (Jackson Laboratories). Oral itraconazole was given twice daily on weekdays and once daily on weekends. ATO was given i.p. on a once-daily schedule.

Medulloblastoma Allograft Models

A parental murine MB model, expressing wild-type SMO, was derived from spontaneous, intracranial MB from $Ptch^{+/-}$; $p53^{-/-}$ mice and maintained as subcutaneous hindflank allografts in athymic nude mice. GDC-0449-resistant allografts expressing SMO^{D477G} (SG274) were derived from parental allografts as previously described (Yauch et al., 2009). Hindflank or orthotopic xenograft models were generated from either parental or SG274 tissues.

Medulloblastoma Culture and Proliferation Assays

MB tumorsphere cultures were derived from either parental or SG274 hind-flank allografts using previously described methods (Shi et al., 2011). Tumorsphere proliferation was quantified by MTS assay following a 96 hr treatment to the various drugs using exposure CellTiter 96 AQ_{ueous} One Solution Cell Proliferation Assay (Promega).

Quantitative PCR of *Gli1* and *Gli2* Transcripts in Medulloblastoma Systems

Established MB tumorspheres were treated for 24 hr with the various drugs. Tissue from tumor-bearing mice were treated for 3 days and harvested 4 hr after the last dose. Relative mRNA was quantified using TaqMan gene probes for *Actin*, *Gli1*, and *Gli2* as previously described (Shi et al., 2011), and reported as fold induction relative to control samples using the ΔΔCt ($2^{-\Delta\Delta Ct}$) method with actin as an internal control.

SUPPLEMENTAL INFORMATION

Supplemental Information includes five figures, four tables, and Supplemental Experimental Procedures and can be found with this article online at http://dx.doi.org/10.1016/j.ccr.2012.11.017.

ACKNOWLEDGMENTS

This research was supported in part by grants from the Virginia and D.K. Ludwig Fund (to G.J.R.), SPARK at Stanford University (to P.A.B.), National Institutes of Health SPORE P50-CA058184, the Flight Attendant Medical Research Institute, and the Burroughs Wellcome Fund (to C.M.R.). P.A.B. is an investigator of the Howard Hughes Medical Institute.

Received: March 14, 2012
Revised: August 27, 2012
Accepted: November 28, 2012
Published: January 3, 2013

REFERENCES

Aftab, B.T., Dobromilskaya, I., Liu, J.O., and Rudin, C.M. (2011). Itraconazole inhibits angiogenesis and tumor growth in non-small cell lung cancer. Cancer Res. *71*, 6764–6772.

Aszterbaum, M., Rothman, A., Johnson, R.L., Fisher, M., Xie, J., Bonifas, J.M., Zhang, X., Scott, M.P., and Epstein, E.H., Jr. (1998). Identification of mutations in the human PATCHED gene in sporadic basal cell carcinomas and in patients with the basal cell nevus syndrome. J. Invest. Dermatol. *110*, 885–888.

Beachy, P.A., Karhadkar, S.S., and Berman, D.M. (2004). Tissue repair and stem cell renewal in carcinogenesis. Nature *432*, 324–331.

Beauchamp, E., Bulut, G., Abaan, O., Chen, K., Merchant, A., Matsui, W., Endo, Y., Rubin, J.S., Toretsky, J., and Uren, A. (2009). GLI1 is a direct transcriptional target of EWS-FLI1 oncoprotein. J. Biol. Chem. *284*, 9074–9082.

Beauchamp, E.M., Ringer, L., Bulut, G., Sajwan, K.P., Hall, M.D., Lee, Y.C., Peaceman, D., Ozdemirli, M., Rodriguez, O., Macdonald, T.J., et al. (2011). Arsenic trioxide inhibits human cancer cell growth and tumor development in mice by blocking Hedgehog/GLI pathway. J. Clin. Invest. *121*, 148–160.

Berman, D.M., Karhadkar, S.S., Hallahan, A.R., Pritchard, J.I., Eberhart, C.G., Watkins, D.N., Chen, J.K., Cooper, M.K., Taipale, J., Olson, J.M., and Beachy, P.A. (2002). Medulloblastoma growth inhibition by hedgehog pathway blockade. Science *297*, 1559–1561.

Buonamici, S., Williams, J., Morrissey, M., Wang, A., Guo, R., Vattay, A., Hsiao, K., Yuan, J., Green, J., Ospina, B., et al. (2010). Interfering with resistance to smoothened antagonists by inhibition of the PI3K pathway in medulloblastoma. Sci. Transl. Med. *2*, 51ra70.

Chen, J.K., Taipale, J., Cooper, M.K., and Beachy, P.A. (2002). Inhibition of Hedgehog signaling by direct binding of cyclopamine to Smoothened. Genes Dev. *16*, 2743–2748.

Cho, Y.J., Tsherniak, A., Tamayo, P., Santagata, S., Ligon, A., Greulich, H., Berhoukim, R., Amani, V., Goumnerova, L., Eberhart, C.G., et al. (2011). Integrative genomic analysis of medulloblastoma identifies a molecular subgroup that drives poor clinical outcome. J. Clin. Oncol. *29*, 1424–1430.

Chong, C.R., Xu, J., Lu, J., Bhat, S., Sullivan, D.J., Jr., and Liu, J.O. (2007). Inhibition of angiogenesis by the antifungal drug itraconazole. ACS Chem. Biol. *2*, 263–270.

Cooper, M.K., Porter, J.A., Young, K.E., and Beachy, P.A. (1998). Teratogen-mediated inhibition of target tissue response to Shh signaling. Science *280*, 1603–1607.

Corbit, K.C., Aanstad, P., Singla, V., Norman, A.R., Stainier, D.Y., and Reiter, J.F. (2005). Vertebrate Smoothened functions at the primary cilium. Nature *437*, 1018–1021.

Cully, M., You, H., Levine, A.J., and Mak, T.W. (2006). Beyond PTEN mutations: the PI3K pathway as an integrator of multiple inputs during tumorigenesis. Nat. Rev. Cancer *6*, 184–192.

de Thé, H., Chomienne, C., Lanotte, M., Degos, L., and Dejean, A. (1990). The t(15;17) translocation of acute promyelocytic leukaemia fuses the retinoic acid receptor alpha gene to a novel transcribed locus. Nature *347*, 558–561.

de Thé, H., Lavau, C., Marchio, A., Chomienne, C., Degos, L., and Dejean, A. (1991). The PML-RAR alpha fusion mRNA generated by the t(15;17) translocation in acute promyelocytic leukemia encodes a functionally altered RAR. Cell *66*, 675–684.

Dijkgraaf, G.J., Alicke, B., Weinmann, L., Januario, T., West, K., Modrusan, Z., Burdick, D., Goldsmith, R., Robarge, K., Sutherlin, D., et al. (2011). Small molecule inhibition of GDC-0449 refractory smoothened mutants and downstream mechanisms of drug resistance. Cancer Res. *71*, 435–444.

Dwyer, J.R., Sever, N., Carlson, M., Nelson, S.F., Beachy, P.A., and Parhami, F. (2007). Oxysterols are novel activators of the hedgehog signaling pathway in pluripotent mesenchymal cells. J. Biol. Chem. *282*, 8959–8968.

Ellison, D.W., Kocak, M., Dalton, J., Megahed, H., Lusher, M.E., Ryan, S.L., Zhao, W., Nicholson, S.L., Taylor, R.E., Bailey, S., and Clifford, S.C. (2011). Definition of disease-risk stratification groups in childhood medulloblastoma using combined clinical, pathologic, and molecular variables. J. Clin. Oncol. *29*, 1400–1407.

Emadi, A., and Gore, S.D. (2010). Arsenic trioxide - An old drug rediscovered. Blood Rev. *24*, 191–199.

Epstein, E.H. (2008). Basal cell carcinomas: attack of the hedgehog. Nat. Rev. Cancer *8*, 743–754.

Gabay, L., Lowell, S., Rubin, L.L., and Anderson, D.J. (2003). Deregulation of dorsoventral patterning by FGF confers trilineage differentiation capacity on CNS stem cells in vitro. Neuron *40*, 485–499.

Gailani, M.R., Bale, S.J., Leffell, D.J., DiGiovanna, J.J., Peck, G.L., Poliak, S., Drum, M.A., Pastakia, B., McBride, O.W., Kase, R., et al. (1992). Developmental defects in Gorlin syndrome related to a putative tumor suppressor gene on chromosome 9. Cell *69*, 111–117.

Gailani, M.R., Ståhle-Bäckdahl, M., Leffell, D.J., Glynn, M., Zaphiropoulos, P.G., Pressman, C., Undén, A.B., Dean, M., Brash, D.E., Bale, A.E., and Toftgård, R. (1996). The role of the human homologue of Drosophila patched in sporadic basal cell carcinomas. Nat. Genet. *14*, 78–81.

Goodrich, L.V., Milenković, L., Higgins, K.M., and Scott, M.P. (1997). Altered neural cell fates and medulloblastoma in mouse patched mutants. Science *277*, 1109–1113.

Gorlin, R.J. (1987). Nevoid basal-cell carcinoma syndrome. Medicine (Baltimore) *66*, 98–113.

Hahn, H., Wicking, C., Zaphiropoulous, P.G., Gailani, M.R., Shanley, S., Chidambaram, A., Vorechovsky, I., Holmberg, E., Unden, A.B., Gillies, S., et al. (1996). Mutations of the human homolog of Drosophila patched in the nevoid basal cell carcinoma syndrome. Cell *85*, 841–851.

Jefferson, E. (2012). FDA approves new treatment for most common type of skin cancer (http://www.fda.gov/NewsEvents/Newsroom/PressAnnouncements/ucm289545.htm).

Johnson, R.L., Rothman, A.L., Xie, J., Goodrich, L.V., Bare, J.W., Bonifas, J.M., Quinn, A.G., Myers, R.M., Cox, D.R., Epstein, E.H., Jr., and Scott, M.P.

(1996). Human homolog of patched, a candidate gene for the basal cell nevus syndrome. Science *272*, 1668–1671.

Joo, J., Christensen, L., Warner, K., States, L., Kang, H.G., Vo, K., Lawlor, E.R., and May, W.A. (2009). GLI1 is a central mediator of EWS/FLI1 signaling in Ewing tumors. PLoS ONE *4*, e7608.

Keeler, R.F., and Binns, W. (1966). Teratogenic compounds of Veratrum californicum (Durand). I. Preparation and characterization of fractions and alkaloids for biologic testing. Can. J. Biochem. *44*, 819–828.

Keeler, R.F., and Binns, W. (1968). Teratogenic compounds of Veratrum californicum (Durand). V. Comparison of cyclopian effects of steroidal alkaloids from the plant and structurally related compounds from other sources. Teratology *1*, 5–10.

Kim, J., Kato, M., and Beachy, P.A. (2009). Gli2 trafficking links Hedgehog-dependent activation of Smoothened in the primary cilium to transcriptional activation in the nucleus. Proc. Natl. Acad. Sci. USA *106*, 21666–21671.

Kim, J., Lee, J.J., Kim, J., Gardner, D., and Beachy, P.A. (2010a). Arsenic antagonizes the Hedgehog pathway by preventing ciliary accumulation and reducing stability of the Gli2 transcriptional effector. Proc. Natl. Acad. Sci. USA *107*, 13432–13437.

Kim, J., Tang, J.Y., Gong, R., Kim, J., Lee, J.J., Clemons, K.V., Chong, C.R., Chang, K.S., Fereshteh, M., Gardner, D., et al. (2010b). Itraconazole, a commonly used antifungal that inhibits Hedgehog pathway activity and cancer growth. Cancer Cell *17*, 388–399.

Lallemand-Breitenbach, V., Jeanne, M., Benhenda, S., Nasr, R., Lei, M., Peres, L., Zhou, J., Zhu, J., Raught, B., and de Thé, H. (2008). Arsenic degrades PML or PML-RARalpha through a SUMO-triggered RNF4/ubiquitin-mediated pathway. Nat. Cell Biol. *10*, 547–555.

Lamb, J.P., Engers, D.W., Niswender, C.M., Rodriguez, A.L., Venable, D.F., Conn, P.J., and Lindsley, C.W. (2011). Discovery of molecular switches within the ADX-47273 mGlu5 PAM scaffold that modulate modes of pharmacology to afford potent mGlu5 NAMs, PAMs and partial antagonists. Bioorg. Med. Chem. Lett. *21*, 2711–2714.

Lee, M.J., Hatton, B.A., Villavicencio, E.H., Khanna, P.C., Friedman, S.D., Ditzler, S., Pullar, B., Robison, K., White, K.F., Tunkey, C., et al. (2012). Hedgehog pathway inhibitor saridegib (IPI-926) increases lifespan in a mouse medulloblastoma model. Proc. Natl. Acad. Sci. USA *109*, 7859–7864.

Maity, T., Fuse, N., and Beachy, P.A. (2005). Molecular mechanisms of Sonic hedgehog mutant effects in holoprosencephaly. Proc. Natl. Acad. Sci. USA *102*, 17026–17031.

Mann, K.K., Colombo, M., and Miller, W.H., Jr. (2008). Arsenic trioxide decreases AKT protein in a caspase-dependent manner. Mol. Cancer Ther. *7*, 1680–1687.

Mao, J., Ligon, K.L., Rakhlin, E.Y., Thayer, S.P., Bronson, R.T., Rowitch, D., and McMahon, A.P. (2006). A novel somatic mouse model to survey tumorigenic potential applied to the Hedgehog pathway. Cancer Res. *66*, 10171–10178.

Monje, M., Beachy, P.A., and Fisher, P.G. (2011). Hedgehogs, flies, Wnts and MYCs: the time has come for many things in medulloblastoma. J. Clin. Oncol. *29*, 1395–1398.

Nacev, B.A., Grassi, P., Dell, A., Haslam, S.M., and Liu, J.O. (2011). The antifungal drug itraconazole inhibits vascular endothelial growth factor receptor 2 (VEGFR2) glycosylation, trafficking and signaling in endothelial cells. J. Biol. Chem. *286*, 44045–44056.

Nachtergaele, S., Mydock, L.K., Krishnan, K., Rammohan, J., Schlesinger, P.H., Covey, D.F., and Rohatgi, R. (2012). Oxysterols are allosteric activators of the oncoprotein Smoothened. Nat. Chem. Biol. *8*, 211–220.

Northcott, P.A., Korshunov, A., Witt, H., Hielscher, T., Eberhart, C.G., Mack, S., Bouffet, E., Clifford, S.C., Hawkins, C.E., French, P., et al. (2011). Medulloblastoma comprises four distinct molecular variants. J. Clin. Oncol. *29*, 1408–1414.

Ocbina, P.J., and Anderson, K.V. (2008). Intraflagellar transport, cilia, and mammalian Hedgehog signaling: analysis in mouse embryonic fibroblasts. Dev. Dyn. *237*, 2030–2038.

Pan, S., Wu, X., Jiang, J., Gao, W., Wan, Y., Cheng, D., Han, D., Liu, J., Englund, N.P., Wang, Y., et al. (2010). Discovery of NVP-LDE225, a potent and selective Smoothened antagonist. ACS Med. Chem. Lett. *1*, 130–134.

Read, T.A., Fogarty, M.P., Markant, S.L., McLendon, R.E., Wei, Z., Ellison, D.W., Febbo, P.G., and Wechsler-Reya, R.J. (2009). Identification of CD15 as a marker for tumor-propagating cells in a mouse model of medulloblastoma. Cancer Cell *15*, 135–147.

Redondo-Muñoz, J., Escobar-Díaz, E., Hernández Del Cerro, M., Pandiella, A., Terol, M.J., García-Marco, J.A., and García-Pardo, A. (2010). Induction of B-chronic lymphocytic leukemia cell apoptosis by arsenic trioxide involves suppression of the phosphoinositide 3-kinase/Akt survival pathway via c-jun-NH2 terminal kinase activation and PTEN upregulation. Clin. Cancer Res. *16*, 4382–4391.

Reifenberger, J., Wolter, M., Weber, R.G., Megahed, M., Ruzicka, T., Lichter, P., and Reifenberger, G. (1998). Missense mutations in SMOH in sporadic basal cell carcinomas of the skin and primitive neuroectodermal tumors of the central nervous system. Cancer Res. *58*, 1798–1803.

Robarge, K.D., Brunton, S.A., Castanedo, G.M., Cui, Y., Dina, M.S., Goldsmith, R., Gould, S.E., Guichert, O., Gunzner, J.L., Halladay, J., et al. (2009). GDC-0449-a potent inhibitor of the hedgehog pathway. Bioorg. Med. Chem. Lett. *19*, 5576–5581.

Rodriguez, A.L., Nong, Y., Sekaran, N.K., Alagille, D., Tamagnan, G.D., and Conn, P.J. (2005). A close structural analog of 2-methyl-6-(phenylethynyl)-pyridine acts as a neutral allosteric site ligand on metabotropic glutamate receptor subtype 5 and blocks the effects of multiple allosteric modulators. Mol. Pharmacol. *68*, 1793–1802.

Rodriguez, A.L., Grier, M.D., Jones, C.K., Herman, E.J., Kane, A.S., Smith, R.L., Williams, R., Zhou, Y., Marlo, J.E., Days, E.L., et al. (2010). Discovery of novel allosteric modulators of metabotropic glutamate receptor subtype 5 reveals chemical and functional diversity and in vivo activity in rat behavioral models of anxiolytic and antipsychotic activity. Mol. Pharmacol. *78*, 1105–1123.

Rohatgi, R., Milenkovic, L., and Scott, M.P. (2007). Patched1 regulates hedgehog signaling at the primary cilium. Science *317*, 372–376.

Romer, J.T., Kimura, H., Magdaleno, S., Sasai, K., Fuller, C., Baines, H., Connelly, M., Stewart, C.F., Gould, S., Rubin, L.L., and Curran, T. (2004). Suppression of the Shh pathway using a small molecule inhibitor eliminates medulloblastoma in Ptc1(+/-)p53(-/-) mice. Cancer Cell *6*, 229–240.

Rowley, J.D., Golomb, H.M., and Dougherty, C. (1977). 15/17 translocation, a consistent chromosomal change in acute promyelocytic leukaemia. Lancet *1*, 549–550.

Rudin, C.M., Hann, C.L., Laterra, J., Yauch, R.L., Callahan, C.A., Fu, L., Holcomb, T., Stinson, J., Gould, S.E., Coleman, B., et al. (2009). Treatment of medulloblastoma with hedgehog pathway inhibitor GDC-0449. N. Engl. J. Med. *361*, 1173–1178.

Shi, W., Nacev, B.A., Aftab, B.T., Head, S., Rudin, C.M., and Liu, J.O. (2011). Itraconazole side chain analogues: structure-activity relationship studies for inhibition of endothelial cell proliferation, vascular endothelial growth factor receptor 2 (VEGFR2) glycosylation, and hedgehog signaling. J. Med. Chem. *54*, 7363–7374.

Shin, K., Lee, J., Guo, N., Kim, J., Lim, A., Qu, L., Mysorekar, I.U., and Beachy, P.A. (2011). Hedgehog/Wnt feedback supports regenerative proliferation of epithelial stem cells in bladder. Nature *472*, 110–114.

Taipale, J., Chen, J.K., Cooper, M.K., Wang, B., Mann, R.K., Milenkovic, L., Scott, M.P., and Beachy, P.A. (2000). Effects of oncogenic mutations in Smoothened and Patched can be reversed by cyclopamine. Nature *406*, 1005–1009.

Tang, J.Y., Xiao, T.Z., Oda, Y., Chang, K.S., Shpall, E., Wu, A., So, P.L., Hebert, J., Bikle, D., and Epstein, E.H., Jr. (2011). Vitamin D3 inhibits hedgehog signaling and proliferation in murine Basal cell carcinomas. Cancer Prev. Res. (Phila.) *4*, 744–751.

Tao, H., Jin, Q., Koo, D.I., Liao, X., Englund, N.P., Wang, Y., Ramamurthy, A., Schultz, P.G., Dorsch, M., Kelleher, J., and Wu, X. (2011). Small molecule antagonists in distinct binding modes inhibit drug-resistant mutant of smoothened. Chem. Biol. *18*, 432–437.

Teglund, S., and Toftgård, R. (2010). Hedgehog beyond medulloblastoma and basal cell carcinoma. Biochim. Biophys. Acta *1805*, 181–208.

Tremblay, M.R., Lescarbeau, A., Grogan, M.J., Tan, E., Lin, G., Austad, B.C., Yu, L.C., Behnke, M.L., Nair, S.J., Hagel, M., et al. (2009). Discovery of a potent and orally active hedgehog pathway antagonist (IPI-926). J. Med. Chem. *52*, 4400–4418.

Varjosalo, M., and Taipale, J. (2008). Hedgehog: functions and mechanisms. Genes Dev. *22*, 2454–2472.

Varjosalo, M., Li, S.P., and Taipale, J. (2006). Divergence of hedgehog signal transduction mechanism between Drosophila and mammals. Dev. Cell *10*, 177–186.

Wang, E.J., Lew, K., Casciano, C.N., Clement, R.P., and Johnson, W.W. (2002). Interaction of common azole antifungals with P glycoprotein. Antimicrob. Agents Chemother. *46*, 160–165.

Ward, R.J., Lee, L., Graham, K., Satkunendran, T., Yoshikawa, K., Ling, E., Harper, L., Austin, R., Nieuwenhuis, E., Clarke, I.D., et al. (2009). Multipotent CD15+ cancer stem cells in patched-1-deficient mouse medulloblastoma. Cancer Res. *69*, 4682–4690.

Wood, M.R., Hopkins, C.R., Brogan, J.T., Conn, P.J., and Lindsley, C.W. (2011). "Molecular switches" on mGluR allosteric ligands that modulate modes of pharmacology. Biochemistry *50*, 2403–2410.

Xie, J., Murone, M., Luoh, S.M., Ryan, A., Gu, Q., Zhang, C., Bonifas, J.M., Lam, C.W., Hynes, M., Goddard, A., et al. (1998). Activating Smoothened mutations in sporadic basal-cell carcinoma. Nature *391*, 90–92.

Xu, J., Dang, Y., Ren, Y.R., and Liu, J.O. (2010). Cholesterol trafficking is required for mTOR activation in endothelial cells. Proc. Natl. Acad. Sci. USA *107*, 4764–4769.

Yauch, R.L., Dijkgraaf, G.J., Alicke, B., Januario, T., Ahn, C.P., Holcomb, T., Pujara, K., Stinson, J., Callahan, C.A., Tang, T., et al. (2009). Smoothened mutation confers resistance to a Hedgehog pathway inhibitor in medulloblastoma. Science *326*, 572–574.

Zhang, X.W., Yan, X.J., Zhou, Z.R., Yang, F.F., Wu, Z.Y., Sun, H.B., Liang, W.X., Song, A.X., Lallemand-Breitenbach, V., Jeanne, M., et al. (2010). Arsenic trioxide controls the fate of the PML-RARalpha oncoprotein by directly binding PML. Science *328*, 240–243.

Zhu, Q., Zhang, J.W., Zhu, H.Q., Shen, Y.L., Flexor, M., Jia, P.M., Yu, Y., Cai, X., Waxman, S., Lanotte, M., et al. (2002). Synergic effects of arsenic trioxide and cAMP during acute promyelocytic leukemia cell maturation subtends a novel signaling cross-talk. Blood *99*, 1014–1022.

Zwerner, J.P., Joo, J., Warner, K.L., Christensen, L., Hu-Lieskovan, S., Triche, T.J., and May, W.A. (2008). The EWS/FLI1 oncogenic transcription factor deregulates GLI1. Oncogene *27*, 3282–3291.